Inorganic Chemistry

Article

pubs.acs.org/IC

Tetradihydrobenzoquinonate and Tetrachloranilate Zr(IV) Complexes: Single-Crystal-to-Single-Crystal Phase Transition and Open-Framework Behavior for $K_4Zr(DBQ)_4$

Inhar Imaz,[†,⊥] Georges Mouchaham,[‡,§] Nans Roques,[‡,§] Stéphane Brandès,[∥] and Jean-Pascal Sutter*[,†,‡,§]

[†]CNRS, Université de Bordeaux, ICMCB, 87 Av. Doc. A. Schweitzer, 33608 Pessac, France

[‡]CNRS, LCC (Laboratoire de Chimie de Coordination), 205 route de Narbonne, F-31077 Toulouse, France

[§]Université de Toulouse, UPS, INPT, LCC, F-31077 Toulouse, France

[∥]ICMUB (Institut de Chimie Moléculaire de l'Université de Bourgogne), UMR 6302 CNRS, Université de Bourgogne, 21078 Dijon, France

[⊥]Esfera UAB, ICN CSIC, CIN2, Bellaterra 08193, Spain

Supporting Information

ABSTRACT: The molecular complexes $K_4[Zr(DBQ)_4]$ and $K_4[Zr(CA)_4]$, where DBQ^{2-} and CA^{2-} stand respectively for deprotonated dihydroxybenzoquinone and chloranilic acid, are reported. The anionic metal complexes consist of Zr(IV) surrounded by four O,O-chelating ligands. Besides the preparation and crystal structures for the two complexes, we show that in the solid state the DBQ complex forms a 3-D open framework (with 22% accessible volume) that undergoes a crystal-to-crystal phase transition to a compact structure upon guest molecule release. This process is reversible. In the presence of H_2O, CO_2, and other small molecules, the framework opens and accommodates guest molecules. CO_2 adsorption isotherms show that the framework breathing occurs only when a slight gas pressure is applied. Crystal structures for both the hydrated and guest free phases of $K_4[Zr(DBQ)_4]$ have been investigated.

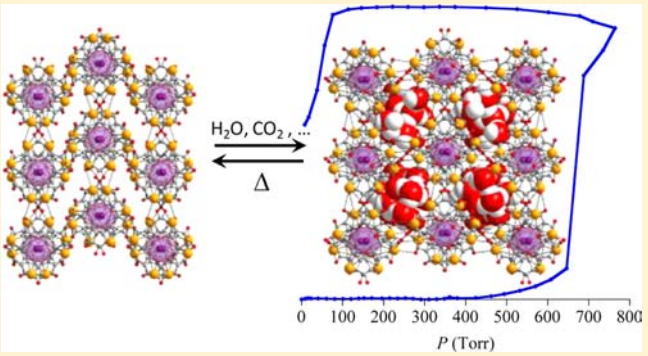

INTRODUCTION

The molecular building block approach is one of the most efficient and widely used strategies for the construction of heterometallic coordination polymers. It relies upon preformed metal complexes able to act as ligands for another metal ion. Typical examples of such metallo-ligands are molecular oxalate complexes for which the oxalate ligand, $C_2O_4^{2-}$, is bound by two of its oxygen atoms to the central metal ion while the two remaining oxygens are available for an additional coordination. By subsequent reaction with a metal ion the oxalate is acting as bridging ligand between two metal centers. Many different monometallic−oxalate complexes containing two, three, and even four oxalate groups have been described[1] and used for the preparation of heterometallic materials.[2] We have been investigating tetraoxalato complexes $[M(C_2O_4)_4]^{4-}$ ($M = Zr^{IV}$, U^{IV}) as building units for the construction of open-framework materials. These complexes can act as tetrahedral nodes likely to induce 3D diamond-like topologies for the final crystalline architecture.[3] Additionally, their negatively charged oxygen-atoms can be involved as H-acceptors in conjunction with H-donor units for the construction of H-bonded networks.[4] Supramolecular architectures with interesting sorption properties and/or porosity have been obtained following these two approaches.[3b,4b,e] For these compounds the oxalate moiety acts as spacer; replacing it by a larger linker could directly contribute to enlarging the porosity of the materials. This led us to explore the possibility of synthesizing metallo-ligands similar to $[M(C_2O_4]^{4-}$ with larger oxocarbon anions.

Herein we report on two such complexes, namely $K_4[Zr(DBQ)_4]$ and $K_4[Zr(CA)_4]$, where DBQ^{2-} and CA^{2-} stand, respectively, for deprotonated dihydroxybenzoquinone and chloranilic acid (Scheme 1). Closely related to oxalate from the point of view of connectivity, charge, and nature of the chelating donor groups, the DBQ^{2-} and CA^{2-} ligands[5] appeared as appropriate alternatives to elaborate tetrasubstituted metallo-ligands. Compared with the oxalate, introduction of a phenyl spacer in between the two O,O-chelating groups increases the distance between bridged metal ions by ca. 2.5 Å. The larger separation between potential H-bond acceptors, i.e., the oxygen atoms coordinated to the central ion (inner-O) and

Received: June 10, 2013
Published: September 26, 2013

Scheme 1. (From Left) Oxalate, Dihydroxybenzoquinonate, and Chloranilate Ligands

those at the periphery of the complex (outer-O atoms), was also of potential interest to improve the control over H-bonded assemblies.[6]

Our choice went for Zr(IV) as metal center because this tetravalent ion was found the lead to metal−organic open-framework materials with remarkable chemical and hydrothermal stabilities,[7] and increased catalytic activities.[8]

Besides the preparation and crystal structures for the two complexes, we show that in solid-state DBQ complex forms a 3-D open framework (with 22% accessible volume) which undergoes a crystal-to-crystal phase transition upon guest molecules release[9] to a compact structure. This process is reversible and in the presence of H_2O, CO_2, and other small molecules the compact phase opens to accommodate these guests. CO_2 adsorption isotherms show that the framework opens only under a slight gas pressure. Crystal structures for both the hydrated and guest free phases have been investigated.

RESULTS AND DISCUSSION

Synthesis. Potassium salts of $[Zr(DBQ)_4]^{4-}$ and $[Zr(CA)_4]^{4-}$ have been synthesized following a sequential methodology directly inspired from the synthesis of $[Zr(C_2O_4)_4]^{4-}$.[10] The synthetic procedure for $[Zr(DBQ)_4]^{4-}$ is briefly described below; the same applies for $[Zr(CA)_4]^{4-}$. Details are given in the Experimental Section. The first step involves the preparation of the $[Zr(DBQ)_2(H_2O)_x]$ neutral complex. This compound is precipitated reacting $ZrOCl_2$ with 2 equiv of H_2DBQ in a water/ethanol mixture. The subsequent addition of 2 equiv of K_2DBQ followed by gentle heating for 2 h, leads to the dissolution of the solid material. The resulting deep red solution affords $\{K_4[Zr(DBQ)_4]\}\cdot 9H_2O$ (**1a** in the following) as a dark red microcrystalline powder in 75% yield upon concentration and cooling. The related procedure with chloranilic acid leads to $\{K_4[Zr(CA)_4]\}\cdot 7H_2O$ (**2** in the following) with 51% yield.

Crystal Structures. Crystallographic data and structure-refinement parameters for **1a**, **1b** (the dehydrated phase of **1a**), and **2** are given in Table 1 and in the Experimental Section. ORTEP plots and selected metric data are provided as Supporting Information. In the following structure descriptions, oxygen atoms of dihydrobenzoquinonate (DBQ^{2-}) and chloranilate (CA^{2-}) ligands are referred to as "internal" (or "inner") oxygen atoms when they are coordinated to zirconium, whereas the other ones are referred to as "external" (or "outer") oxygen atoms.

*$\{K_4[Zr(DBQ)_4]\}\cdot 9H_2O$, **1a**.* Single crystals suitable for X-ray diffraction studies were obtained upon room-temperature slow evaporation of the reaction mixture. Compound **1a**, $\{K_4[Zr$-

Table 1. Crystallographic Data and Structural Refinement Parameters for Compounds 1a, 1b, and 2

compounds	1a	1b	2
empirical formula	$Zr_1C_{24}H_{26}O_{25}K_4$	$Zr_1C_{24}H_8O_{16}K_4$	$Zr_1C_{24}H_{14}Cl_8O_{23}K_4$
formula wt ($g.mol^{-1}$)	962.07	799.92	1191.49
temp (K)	293(2)	373(2)	293(2)
crystal syst	orthorhombic	orthorhombic	monoclinic
space group	*Pbca*	*Pbca*	*P2/c*
a (Å)	17.156(3)	17.340(2)	10.884
b (Å)	20.387(4)	20.333(2)	15.726
c (Å)	20.562(4)	16.515(2)	14.071
α (deg)	90	90	90
β (deg)	90	90	124.0
γ (deg)	90	90	90
volume ($Å^3$)	7192(2)	5823.1(11)	1996.5
Z	8	8	2
density ($g\cdot cm^{-3}$)	1.777	1.825	1.982
absorption coefficient (mm^{-1})	0.864	1.026	1.314
F (000)	3888	3168	1168
θ range for data collection (°)	2.23−26.37	2.35−21.95	2.17−26.31
reflections collected	47607	22989	4050
independent reflections	7342 [*R*(int) = 0.032]	3529 [*R*(int) = 0.036]	4050 [*R*(int) = 0.039]
data/restraints/parameters	7342/6/528	3529/0/401	4050/0/281
goodness-of-fit	1.220	1.242	1.093
refinement on	F^2	F^2	F^2
final *R* indices	*R* = 0.0494	*R* = 0.0527	*R* = 0.0455
	w*R* = 0.1596	w*R* = 0.1418	w*R* = 0.1346
	R_{all} = 0.0601	R_{all} = 0.0828	R_{all} = 0.0638
	wR_2 = 0.1829	wR_2 = 0.2016	wR_2 = 0.1452
largest diff. peak and hole (e $Å^{-3}$)	1.272 and −1.509	1.226 and −1.282	0.637 and −1.654
CCDC no.	943451	943452	943453

dx.doi.org/10.1021/ic401474f | *Inorg. Chem.* 2013, 52, 11237−11243

$(DBQ)_4]\}\cdot 9H_2O$, crystallizes in the orthorhombic *Pbca* space group. Asymmetric unit consists of one $[Zr(DBQ)_4]^{4-}$ anion, four K^+, and nine H_2O molecules (see Figure S1 (Supporting Information) for ORTEP plot); a view of the anionic molecular complex is given in Figure 1. Each Zr(IV) is surrounded by four

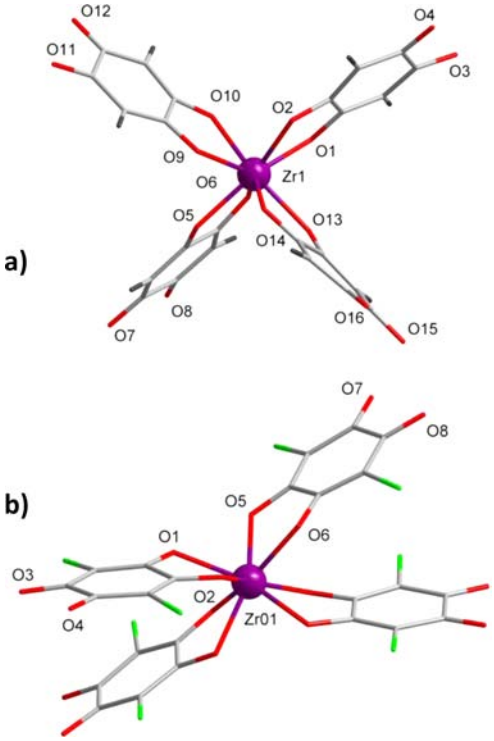

Figure 1. Molecular structures of the anionic complexes (a) $[Zr(DBQ)_4]^{4-}$, **1a**, and (b) $[Zr(CA)_4]^{4-}$, **2**. Selected bond lengths (Å): **1a**: O1−Zr, 2.234(4); O2−Zr, 2.179(4); O5−Zr, 2.183(4); O6−Zr, 2.197(4); O9−Zr, 2.218(4); O10−Zr, 2.188(4); O13−Zr, 2.199(4); O14−Zr, 2.191(3); O1−C1, 1.295(7); O2−C2, 1.300(7); O4−C4, 1.242(7); O5−C7, 1.302(7); O6−C8, 1.305 (7); O7−C11, 1.238(7); O8−C10, 1.239(7); O9−C13, 1.280(7); O10−C14, 1.301(7); O11−C17, 1.253(7); O12−C16, 1.232(7); O13−C19, 1.302(7); O14−C20, 1.314(7); O15−C23, 1.247(7); O16−C22, 1.230(7). **2**: O1−Zr, 2.169(3); O2−Zr, 2.226(3); O1−C1, 1.295(6); O2−C2, 1.292(6); O3−C5, 1.226(6); O4−C4, 1.222(6); O5−C8, 1.293(6); O6−C7, 1.284(5); O7−C10, 1.217(6); O8−C11, 1.224(6).

bidentate DBQ with angles between consecutive DBQ ranging from 88.5 to 105.9°.[11] The C−O and C−C bond lengths are in agreement with a delocalization of the negative charges over the four oxygen atoms of the DBQ ligands as sketched in Scheme 1. Extensive bonding takes place between the $[Zr(DBQ)_4]^{4-}$ units and the potassium cations. Each anion is bound to 12 K^+ (Figure 2a), while each K^+ bridges three different $[Zr(DBQ)_4]^{4-}$ anions to afford a 3D architecture. The K^+ are linked to both internal and external O-atoms to form O−K−O bridges (K···O distances range from 2.61 to 2.99 Å, Table S1, Supporting Information), and their coordination sphere is completed by H_2O molecules (one for K1, K2, and K4; two for K3). As anticipated, the $Zr-O_{int}$ bond lengths are comparable to the ones observed with oxalate ligands,[10] while the $Zr\cdots O_{ext}$ distances are increased to a maximum value of 6.63 Å. Consequently, the spacing between the central Zr and the K atoms linked to external O-atoms of a DBQ ligand reaches up to 9.19 Å. Structure examination along the *a* axis reveals supramolecular chains where $[Zr(DBQ)_4]^{4-}$ units are connected through $O_{int}-K-O_{ext}$ bridges involving K1−4 cations. Interconnection of the chains along *b* (through O−K2−O and O−K4−O bridges) and *c* (through O−K1−O and O−K3−O bridges) affords a 3D architecture showing infinite channels with rectangular apertures of 3 Å × 1 Å (van der Waals radii for K^+ and O atoms have been taken into account) running along the *a* axis (Figure 2). The H_2O molecules coordinated to K^+ are located in these channels, together with guest H_2O molecules which are H-bonded to the coordinated ones. When guest and coordinated H_2O molecules are neglected, the 1D channels endow this material with a total solvent accessible void volume of 22.5% of the cell volume. In absolute terms, it represents a volume of 1620 $Å^3$ per 7192 $Å^3$ of the unit cell.[12]

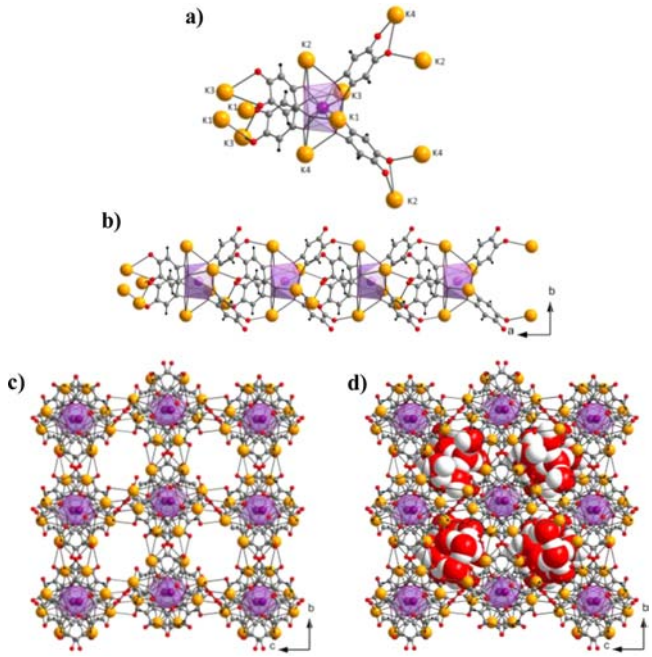

Figure 2. 3D supramolecular architecture of $\{K_4[Zr(DBQ)_4]\}\cdot 9H_2O$ (the Zr polyhedron is depicted in purple): (a) $[Zr(DBQ)_4]^{4-}$ unit connected to 12 K^+ bridging cations. (b) Linear chain running along the *a* axis. (c) 3D architecture resulting from the chains interconnection. (d) H_2O molecules (in space-filling) located in the structure cavities. Color codes: Zr, violet; C, gray; O, red; H, black; K, orange.

*$K_4[Zr(DBQ)_4]$, **1b**.* Upon heating, compound **1a** was found to release its H_2O molecules and undergo a structural phase transition (see below). Performing the experiment on a single crystal of **1a** revealed a single crystal-to-single crystal phase transition to the guest free solid. The structure of the evacuated phase, $K_4[Zr(DBQ)_4]$, **1b**, was determined by X-ray diffraction studies by warming a single crystal of **1a** to 100 °C. Compared to the hydrated phase, the space group (orthorhombic *Pbca*) for **1b** is unchanged and the cell parameters *a* and *b* remain very similar; however, the *c* parameter is shrunk by 20% (Table 1) suggesting a subsidence of the framework along one direction. The asymmetric unit for **1b** consists of one $[Zr(DBQ)_4]^{4-}$ anion and four K^+ (Figure 3 and Figure S2, Supporting Information). The angles between consecutive DBQ ligands in the $[Zr(DBQ)_4]^{4-}$ unit, the K to $[Zr(DBQ)_4]$ connectivity, and the K−O bond lengths and Zr···K distances are almost unchanged as compared to **1a**. However, H_2O departure induces important alterations for O−K−O angles for which the average value of 115.5° observed in **1a** is decreased

dx.doi.org/10.1021/ic401474f | *Inorg. Chem.* 2013, 52, 11237−11243

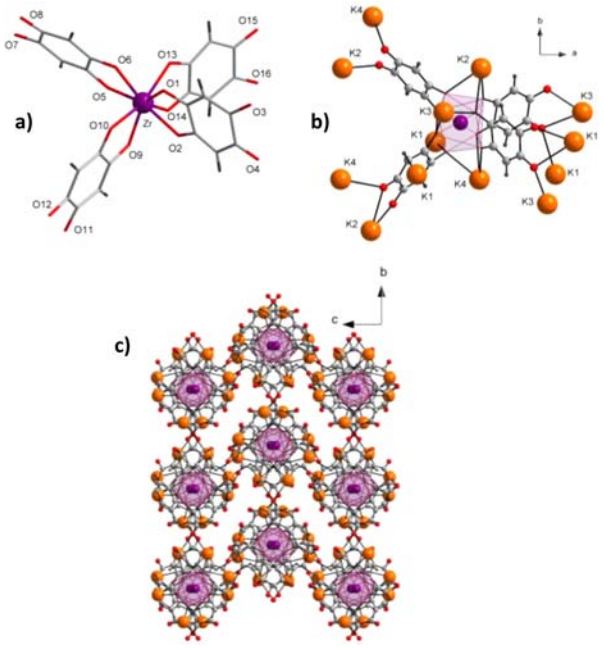

Figure 3. $K_4[Zr(DBQ)_4]$, **1b**: (a) molecular structure of the anionic complex $[Zr(DBQ)_4]$, (b) detail of the coordination to K^+ ions (the Zr polyhedron is depicted in purple), (c) 3D coordination network. Color codes: Zr, violet; C, gray; O, red; H, black; K, orange. Selected bond lengths (Å): O1–Zr1, 2.209(5); O2–Zr1, 2.185(5); O5–Zr1, 2.173(5); O6–Zr1, 2.204(4); O9–Zr1, 2.210(4); O10–Zr1, 2.225(5); O13–Zr1, 2.168(5); O14–Zr1, 2.2535(50); O1–C1, 1.315(8); O2–C2, 1.301(9); O3–C5, 1.24(1); O4–C4, 1.23 (1); O5–C7, 1.309(9); O6–C8, 1.304(8); O7–C11,1.23 (1); O8–C10, 1.23(1); O9–C13, 1.305(8); O10–C14, 1.276(8); O11–C17, 1.22(1); O12–C16, 1.25(1); O13–C19, 1.307(8); O14–C20, 1.298(8); O15–C23, 1.245(8); O16–C22, 1.252(8).

to 110.9° in **1b** (for details related to bond angles variations, see Figure S3, Supporting Information). Structural changes induced by H_2O release are clearly visible in Figure 3c; they are sketched in Scheme 2. The Zr–K chains running along *a* axis

Scheme 2. Schematic Representation of the Crystal Packing Modification during the Reversible Crystal-to-Crystal Transformation between 1a (in Blue) and 1b (in Red)

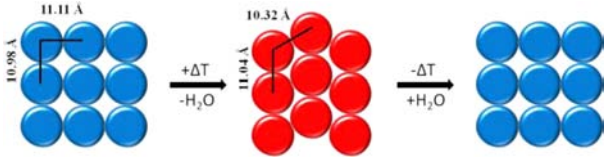

are staggered in *bc* plane for **1b**, whereas they are perfectly aligned with the axis for hydrated phase **1a**. During guest release the array along *c* axis fold up to compensate the volume freed by the H_2O molecules. It can be noticed however, that the Zr···Zr distances between adjacent chains are hardly changed with 9.959(1), 10.315(1), 11.038(1), and 11.077(1) Å for **1b** versus 10.98 Å and 11.11 Å for **1a**. Consequently, cell parameter *a* and *b* are little modified (+1.1% and −0.3%, respectively), while *c* is contracted by 19.7%. The strong contraction along *c* drastically reduces the solvent accessible void volume to become negligible (1.2%, that is a volume of 71 $Å^3$ per 5822.8 $Å^3$ of the unit cell) for **1b**.

Interestingly, the cell parameters corresponding to **1a** were recovered for the single crystal of **1b** after keeping it in air at room temperature for a few hours, thus confirming the reversibility of the structural transition. Further evidence for this has been obtained from powder X-ray diffraction studies (vide infra).

$\{K_4[Zr(CA)_4]\}\cdot 7H_2O$, ***2***. Compound **2** crystallizes in the monoclinic *P*2/c space group. The asymmetric unit consists of half a $[Zr(CA)_4]^{4-}$ anion, two K^+, and three and a half H_2O molecules (see Figure S3 (Supporting Information) for the ORTEP plot and Table S3 (Supporting Information) for metric data). Each Zr(IV) is surrounded by four chloranilate ligands, and each ligand makes a chelate-type coordination to a single Zr ion (Figure 1b). The Zr–O distances are very close to that found for $[Zr(DBQ)_4]^{4-}$, and the C–O and C–C bond lengths are in agreement with a delocalization of the negative charges over the four oxygen atoms of the ligands. The angles between consecutive ligands range from 61.7 to 127.8°. As a result, the $[Zr(CA)_4]^{4-}$ complex appears flattened as compared to $[Zr(DBQ)_4]^{4-}$. Each anionic complex makes coordination interactions (≤3 Å) with eight K^+ cations whereas each K atom bridges two complexes, thus developing to a 2-D coordination polymer (Figure 4). Six H_2O molecules act as ligands for K^+, and one (O3w) is located within the layer.

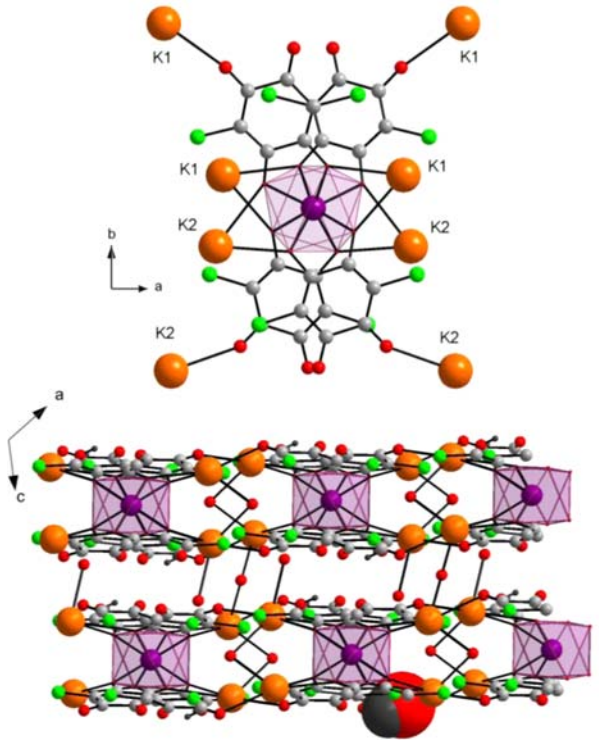

Figure 4. $\{K_4[Zr(CA)_4]\}\cdot 7H_2O$, **2**: (top) detail of the coordination to K^+ ions; (bottom) layer arrangement of the 2D coordination polymer. One noncoordinated H_2O (O3w) is shown in space-filling. Color codes: Zr, violet; C, gray; O, red; H, black; K, orange, Cl, green.

No crystal phase transition was observed for **2** upon water release. The solid turns amorphous when dehydrated, and crystallinity is not recovered when the activated solid is left in air.

Open-Framework Features for 1a. *Stability and Flexibility.* Thermogravimetric analysis performed for **1a** reveals that the H_2O molecules are released under mild conditions

dx.doi.org/10.1021/ic401474f | *Inorg. Chem.* 2013, 52, 11237–11243

while the coordination framework remains stable until 200 °C (Figure S5, Supporting Information). H_2O departure starts already at room temperature and is complete at 120 °C. This is supported by the diffractograms recorded on a powder sample of **1a** at different temperatures (Figure S6, Supporting Information). For $T \geq 80$ °C, only the phase corresponding to the compact structure **1b** is observed. When the dehydrated phase is cooled to 20 °C and kept in air for a few hours the phase corresponding to **1a** is recovered, confirming the reversibility of the H_2O sorption process. Interestingly, when the activated compound **1b** is kept in a N_2 atmosphere the diffractogram collected at 20 °C shows no phase modification (Figure 5).

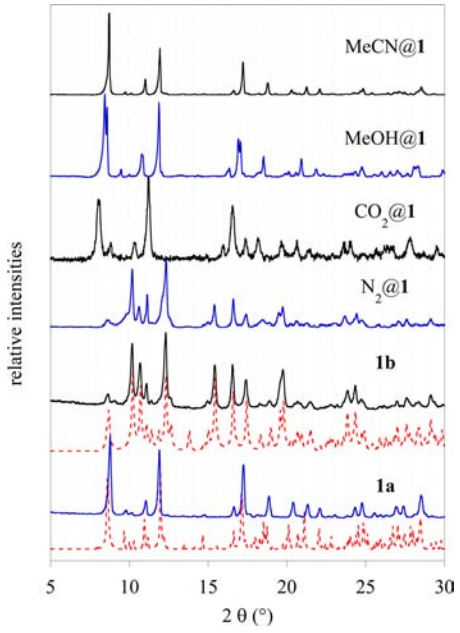

Figure 5. Powder X-ray diffractograms for **1a**, **1b**, and phase obtained with other guest molecules. The dotted plots correspond to the diffraction patterns calculated from the crystal structure data. The experimental diffractogram for **1b** has been recorded at 120 °C. The data for N_2@**1** and CO_2@**1** have been collected from **1b** kept in the corresponding gas atmosphere.

Guest Sorption. The framework of **1b** was found to open in the presence of various small molecules such as CO_2, MeOH, or MeCN. This is evidenced by the PXRD obtained after **1b** (activated **1a**) was put in contact with these molecules. In all cases, a new crystalline phase is found. Such behavior highlights remarkable framework flexibility with in each case a crystal-to-crystal phase transformation. Following the classification proposed by Kitagawa et al., the open-framework architecture **1** thus belongs to the compounds of type 1 of the third generation of solvated solids; i.e., the sample retains its crystalline nature during the sorption process.[13]

Gas sorption isotherms have been recorded for **1b** with different gases (Figure 6). A very small sorption was observed for N_2 at 77 K yielding a surface area of 4 $m^2\ g^{-1}$ (Figure S7, Supporting Information), thus confirming the compact structure of the activated phase **1b**, in agreement with the X-ray data. The same behavior was found with O_2 and CO at 25 °C. However, with CO_2 the framework opens and gas sorption is obtained. The CO_2 sorption isotherms profiles obtained at +25 and −1 °C reveal a progressive increase of the adsorbed

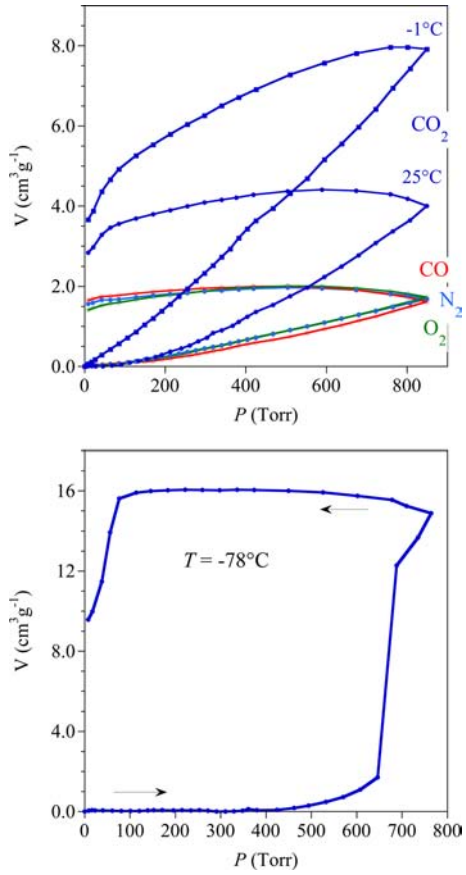

Figure 6. Adsorption isotherms for **1b** (top) of N_2, O_2, CO, and CO_2 at 25 °C (●) and at −1 °C (□, CO_2) and (bottom) of CO_2 at −78 °C.

gas volume with the gas pressure and the desorption legs does not match the adsorption branch, resulting in large hysteresis loops over the whole pressure range. It can be noticed that the variation of the adsorbed volume with pressure is not linear in the lower pressure domain, and the curvature of the isotherm is inverse in respect to an expected Langmuir-type isotherm. Such a behavior is characteristic for a progressive opening of the framework by applying a gas pressure.[14,15] The material does not show a clear isotherm inflection at +25 or −1 °C typical of a structurally dynamic behavior, but this breathing effect is by far more pronounced at lower temperatures (see below).

The rather selective sorption of CO_2 over N_2, O_2 and CO at 25 °C for **1b** is due to the small pore size and selective binding to the walls of the framework by a size-exclusion effect, as revealed by the small pore size shown by X-ray single crystals analysis. This suggests that **1b** can discriminate the gases based mainly on their size (CO_2, 3.3 Å over N_2, 3.64 Å, O_2, 3.46 Å and CO, 3.76 Å) and shape. The isosteric heats of adsorption for **1b** were calculated using the Clausius−Clapeyron equation, and the results are presented in Figure S8, Supporting Information. The heat of adsorption remains between 17 and 20 kJ mol^{-1} at higher loadings, which is in the range of physical adsorption. However, in the lower CO_2 loading region, larger values were obtained suggesting that CO_2 molecules are interacting with the surface potentials of the pore walls. This can be attributed to the partial opening of the framework at lower pressures that endows porosity to the material. The variation of the heat of adsorption is also indicative for the heterogeneity of the adsorption sites.

dx.doi.org/10.1021/ic401474f | Inorg. Chem. 2013, 52, 11237−11243

The isotherm recorded at −78 °C shows a fairly unusual gated adsorption behavior since almost no adsorption takes place until a pressure of ca. 650 Torr, above which a sudden CO_2 uptake is observed to reach 16 $cm^3\ g^{-1}$ (3.1 wt %) at 750 Torr. When the pressure was decreased, the adsorbed volume remained unchanged until P = 0.08 Torr. Such behavior suggests a structural change from a closed- to an open-framework triggered by the CO_2 pressure. This was revealed by XRD under CO_2 atmosphere (see Figure 5) since a shift of the diffraction peaks to lower angles was observed, which is due to the expansion and the opening of the framework. The abrupt adsorption to a maximum volume indicates that the framework-opening process is not progressive but corresponds to a transition from the closed to a porous phase. These features are typical of a breathing material with a gated behavior under a CO_2 atmosphere.[15,16] The marked broad hysteresis loops confirms that the adsorbed CO_2 is not immediately released on reducing the external pressure and is thus trapped within the framework due to attractive CO_2−CO_2 and sorbate−sorbent interactions. It can only be effectively removed at very low pressures. The CO_2 isotherm at 195 K is quite unusual but not unprecedented.[15,16a]

In addition to this qualitative analysis, it is possible to assess the breathing phenomena by calculating the pore volume in the closed form **1b**. By considering that the porosity determined by X-ray analysis is only 1.2%, the cell volume in **1b** is about 0.0066 $cm^3\ g^{-1}$ but the actual adsorption analysis gives 0.029 $cm^3\ g^{-1}$ (16 $cm^3\ g^{-1}$ for the gas) at 750 Torr. These data reveals a significant pore expansion. However, this volume is below the value that can be estimated (0.15 $cm^3\ g^{-1}$) for **1a** without water molecules in the pores. This suggests that the framework is only partially opened with the conditions used; higher gas pressures may well further swell this flexible architecture and expand the space available for guest molecules.

CONCLUDING REMARKS

The preparation of anionic Zr(IV) complexes homologous to the tetraoxalato complex has been achieved with the larger chloralinate and dihydrobenzoquinonate ligands. With respect to the oxalate complexes, these potential metallo-ligands offer the possibility to increase the separation between the two metal ions bridged by the oxycarbon ligands, a desirable feature for the preparation of MOF-type materials. An illustration for this is provided by $K_4[Zr(DBQ]\cdot 9H_2O$ which was found to exhibit an open-framework with a remarkable structural flexibility. The possibility to involve these complexes as H-bond acceptors for the formation of H-bonded porous architectures is in progress.

EXPERIMENTAL SECTION

General Methods. All chemicals were purchased from commercial sources and used as received. All reactions were performed in distilled water and under aerobic conditions. Infrared spectra were recorded with a Perkin-Elmer Spectrum 100 FT-IR spectrometer in the range 4000−600 cm^{-1}. Elemental analyses were performed using a Perkin-Elmer 2400 II, CHNS/O analyzer. TGA measurements have been done on a Perkin-Elmer Diamond TG/DTA instrument. The compounds were heated 1 °C/min between rt and 200 and 10 °C/min above.

$\{K_4[Zr(C_6H_2O_4)_4]\}\cdot 9H_2O$, 1a. Solid K_2CO_3 (552 mg; 4 mmol) was slowly added to a suspension of 2,5-dihydro-1,4-benzoquinone (H_2DBQ; 560 mg; 4 mmol) in H_2O (10 mL), under continuous stirring, to form K_2DBQ. In parallel, an EtOH−H_2O (30/20 mL) solution of H_2DBQ (280 mg; 2 mmol) was added to an aqueous solution (5 mL) of $ZrOCl_2$ (332 mg; 1 mmol). After 30 min of stirring, the K_2DBQ solution was slowly added to the suspension, and the resulting mixture was heated at 80 °C for 2 h. The mixture was then concentrated to ca. 10% of its initial volume under reduced pressure, and the resulting solution was stored at 4 °C for 12 h. Compound **1a** was recovered by filtration as a dark red microcrystalline powder (699 mg; 0.73 mmol; 75%). IR (cm^{-1}): 3356 (m), 2934 (m), 1602 (m), 1526 (s), 1350 (s), 1245 (s), 1133 (m), 1057 (m), 989 (m), 918 (w), 819 (s), 667 (m). Anal. Calcd for $K_4Zr_1C_{24}O_{23}H_{22}$: C, 30.80; H, 1.72. Found: C, 31.06; H, 1.91.

$\{K_4[Zr(C_6Cl_2O_4)_4]\}\cdot 7H_2O$, 2. This compound is prepared according to the same procedure described for **1a** using chloranilic acid instead of 2,5-dihydro-1,4-benzoquinone. Yield: 51% (610 mg; 0.49 mmol). IR (cm^{-1}): 3432 (m), 2969 (w), 1647 (m), 1522 (s), 1352 (s), 1319 (s), 1098 (s), 1010 (m), 886 (w), 845 (m). Anal. Calcd for $C_{24}H_{14}O_{23}Cl_8K_4Zr_1$: C, 23.99; H, 1.17. Found: C, 23.85; H, 0.72.

For both **1a** and **2**, suitable single crystals for X-diffraction studies were obtained following the same procedure working with more diluted solutions and upon room temperature slow evaporation of the final reaction mixture.

Guest Exchange Procedure. The guest molecule exchange was carried out under N_2 atmosphere on the activated **1a**. Typically, a capillary of 0.5 mm diameter containing **1a** was heated to 100 °C under vacuum for 5 h and cooled to rt under N_2 in a sealed Schlenk tube. Eventually, anhydrous solvent (MeOH or MeCN) or CO_2 gas was injected into the capillary and/or the Schlenk tube to obtain MeOH@**1**, MeCN@**1**, and CO_2@**1**, respectively. N_2@**1** is the activated material kept under N_2 without any additive. Three days later, the capillary was taken out and sealed prior to performing powder X-ray diffraction measurements.

Crystallographic Studies. Single-crystal X-ray diffraction data were collected on a Bruker Nonius κ-CDD diffractometer at 293 K for compounds **1a** and **2** and at 373 K for compound **1b**. The diffractometer was equipped with an Oxford Cryosystems Cryostream Cooler Device, and the measurements were performed using graphite-monochromated Mo Kα radiation (λ = 0.71073 Å). The structures were solved by direct methods using SIR92;[17] the refinement and all further calculations were carried out using the SHELXL-97 program within the WinGX package.[18] All non-hydrogen atoms were refined anisotropically. The H atoms have been included in theoretical positions on C6-rings and located by Fourier difference for water molecules, but not refined. Empirical absorption corrections were applied in both cases with SCALEPACK.[19] Potassium atom (K1) in the structure of **2** exhibits a bit higher U_{eq} compared to neighbor atoms, certainly due to a disorder since the data was collected at room temperature. Attempts to define disordered positions were unsuccessfully realized.

The powder X-ray diffraction (PXRD) patterns were recorded on a XPert Pro (θ−θ mode) Panalytical diffractometer with $\lambda(Cu_{K\alpha1,K\alpha2})$ = 1.54059, 1.54439 Å. The high temperature PXRD patterns were recorded on a Philips X-Pert (θ−2θ mode) diffractometer coupled to an Anton Parr oven with heating of 1 °C/min rate. All data were collected in the 5° < 2θ < 50° range, with 0.02 steps and 10 s of exposure.

Sorption Studies. Gas adsorption isotherms were recorded on evacuated materials on a Micromeritics ASAP 2020 analyzer. Samples were previously degassed by heating at 373 K in vacuo (10^{-5} Torr) for 3 h. Specific surface areas were measured by N_2 adsorption measurements performed at 77 K using the Brunauer−Emmet−Teller method (BET) in the relative P/P_0 pressure range from 0.05 to 0.25 assuming a monolayer coverage of N_2 and a cross-sectional area of 16.2 $Å^2$/molecule. Sorption analyses were recorded at 298, 272, and 195 K for CO_2 and 298 K for CO, O_2, and N_2. This allowed calculation of the isosteric heat of adsorption for CO_2 by applying the Clausius−Clapeyron equation

$$\frac{\partial \ln P}{\partial (1/T)} = -\frac{\Delta H}{R}$$

where $-\Delta H$ is the isosteric heat of adsorption, P the pressure, R the gas constant, and T the temperature.

dx.doi.org/10.1021/ic401474f | Inorg. Chem. 2013, 52, 11237−11243

■ ASSOCIATED CONTENT

Supporting Information

ORTEP plots and geometrical data for **1a**, **1b**, and **2**; TGA and PXRD for **1a**, N_2 adsorption isotherm and heat of adsorption of CO_2 for **1b**. This material is available free of charge via the Internet at http://pubs.acs.org. The CIF for compounds **1a**, **1b** and **2** have been deposited at the CCDC (www.ccdc.cam.ac.uk) under reference nos. 943451, 943452, and 943453, respectively.

■ AUTHOR INFORMATION

Corresponding Author

*E-mail: sutter@lcc-toulouse.fr.

Notes

The authors declare no competing financial interest.

■ REFERENCES

(1) Krishnamurty, K. V.; Harris, G. M. *Chem. Rev.* **1961**, *61*, 213−246.

(2) (a) Rao, C. N. R.; Natarajan, S.; Vaidhyanathan, R. *Angew. Chem., Int. Ed.* **2004**, *43*, 1466−96. (b) Clemente-Leon, M.; Coronado, E.; Marti-Gastaldo, C.; Romero, F. M. *Chem. Soc. Rev.* **2011**, *40*, 473−497. (c) Decurtins, S.; Pellaux, R.; Hauser, A.; Von Arx, M. E. Solid state supramolecular chemistry of oxalato-bridged transition-metal compounds with two- and three-dimensional connectivities - structure, magnetism and photophysics. In *Magnetism: A Supramolecular Function*; Kahn, O., Ed.; NATO ASI Series, Ser. C ed.; Kluwer: New York, 1996; Vol. *484*, pp 487−508. (d) Gruselle, M.; Train, C.; Boubekeur, K.; Gredin, P.; Ovanesyan, N. *Coord. Chem. Rev.* **2006**, *250*, 2491−2500. (e) Marinescu, G.; Andruh, M.; Lloret, F.; Julve, M. *Coord. Chem. Rev.* **2011**, *255*, 161−185.

(3) (a) Imaz, I.; Bravic, G.; Sutter, J.-P. *Chem. Commun.* **2005**, 993−5. (b) Imaz, I.; Bravic, G.; Sutter, J.-P. *Dalton Trans* **2005**, 2681−2681.

(4) (a) Imaz, I.; Thillet, A.; Sutter, J.-P. *Cryst. Growth Des.* **2007**, *7*, 1753−61. (b) Mouchaham, G.; Roques, N.; Brandès, S.; Duhayon, C.; Sutter, J.-P. *Cryst. Growth Des.* **2011**, *11*, 5424−5433. (c) Mouchaham, G.; Roques, N.; Imaz, I.; Duhayon, C.; Sutter, J.-P. *Cryst. Growth Des.* **2010**, *10*, 4906−4916. (d) Mouchaham, G.; Roques, N.; Kaiba, A.; Guionneau, P.; Sutter, J.-P. *CrystEngComm* **2010**, *12*, 3496−3498. (e) Thétiot, F.; Duhayon, C.; Venkatakrishnan, T. S.; Sutter, J.-P. *Cryst. Growth Des.* **2008**, *8*, 1870−1877.

(5) (a) Abrahams, B. F.; Coleiro, J.; Hoskins, B. F.; Robson, R. *Chem. Commun.* **1996**, 603−604. (b) Robson, R. *Dalton Trans.* **2000**, 3735−3744. (c) Kawata, S.; Kumagai, H.; Adachi, K.; Kitagawa, S. *Dalton Trans.* **2000**, 2409−2417. (d) Kawahara, M.; Kabir Md., K.; Yamada, K.; Adachi, K.; Kumagai, H.; Narumi, Y.; Kindo, K.; Kitagawa, S.; Kawata, S. *Inorg. Chem.* **2004**, *43*, 92−100. (e) Min, K. S.; DiPasquale, A. G.; Golen, J. A.; Rheingold, A. L.; Miller, J. S. *J. Am. Chem. Soc.* **2007**, *129*, 2360−8. (f) Abrahams, B. F.; Hudson, T. A.; McCormick, L. J.; Robson, R. *Cryst. Growth Des.* **2011**, *11*, 2717−2720 and references therein.

(6) Mouchaham, G.; Roques, N.; Duhayon, C.; Imaz, I.; Sutter, J.-P. *New J. Chem.* **2013**, DOI: 10.1039/c3nj00520h.

(7) (a) Cavka, J. H.; Jakobsen, S.; Olsbye, U.; Guillou, N.; Lamberti, C.; Bordiga, S.; Lillerud, K. P. *J. Am. Chem. Soc.* **2008**, *130*, 13850−13851. (b) Guillerm, V.; Ragon, F.; Dan-Hardi, M.; Devic, T.; Vishnuvarthan, M.; Campo, B.; Vimont, A.; Clet, G.; Yang, Q.; Maurin, G.; Férey, G.; Vittadini, A.; Gross, S.; Serre, C. *Angew. Chem., Int. Ed.* **2012**, *51*, 9267−9271. (c) Low, J. J.; Benin, A. I.; Jakubczak, P.; Abrahamian, J. F.; Faheem, S. A.; Willis, R. R. *J. Am. Chem. Soc.* **2009**, *131*, 15834−15842.

(8) (a) Vermoortele, F.; Ameloot, R.; Vimont, A.; Serre, C.; De Vos, D. E. *Chem. Commun.* **2011**, *47*, 1521−1523. (b) Vermoortele, F.; Bueken, B.; Le Bars, G.; Van de Voorde, B.; Vandichel, M.; Houthoofd, K.; Vimont, A.; Daturi, M.; Waroquier, M.; Van Speybroeck, V.; Kirschhock, C.; De Vos, D. E. *J. Am. Chem. Soc.* **2013**, *135*, 11465−11468.

(9) (a) Beauvais, L. G.; Long, J. R. *J. Am. Chem. Soc.* **2002**, *124*, 12096−7. (b) Tian, J.; Saraf, L. V.; Schwenzer, B.; Taylor, S. M.; Brechin, E. K.; Liu, J.; Dalgarno, S. J.; Thallapally, P. K. *J. Am. Chem. Soc.* **2012**, *134*, 9581−9584. (c) Zeng, M.-H.; Feng, X.-L.; Chen, X.-M. *Dalton Trans* **2004**, 2217−23. (d) Ferey, G. *Z. Anorg. Allg. Chem.* **2012**, *638*, 1897. (e) Datcu, A.; Roques, N.; Jubera, V.; Maspoch, D.; Fontrodona, X.; Wurst, K.; Imaz, I.; Mouchaham, G.; Sutter, J.-P.; Rovira, C.; Veciana, J. *Chem.—Eur. J.* **2012**, *18*, 152−162. (f) Milon, J.; Guionneau, P.; Duhayon, C.; Sutter, J.-P. *New J. Chem.* **2011**, *35*, 1211−1218.

(10) Kojic-Prodic, B.; Ruzic-Toros, Z.; Sljukic, M. *Acta Crystallogr.* **1978**, *B34*, 2002−2.

(11) Note: These angles correspond to X−Zr−X angles where X is a fictive atom located at the oxygen atoms median point for each DBQ ligand.

(12) (a) Spek, A. L., *PLATON, A Multipurpose Crystallographic Tool*; Utrech University: Utrecht (The Netherlands), 2001. (b) Spek, A. L. *J. Appl. Crystallogr.* **2003**, *36*, 7−13.

(13) Kitagawa, S.; Kitaura, R.; Noro, S. *Angew. Chem., Int. Ed.* **2004**, *43*, 2334−75.

(14) (a) Bourrely, S.; Llewellyn, P. L.; Serre, C.; Millange, F.; Loiseau, T.; Férey, G. *J. Am. Chem. Soc.* **2007**, *127*, 13519−21. (b) Serre, C.; Bourelly, S.; Vimont, A.; N.A., R.; Maurin, G.; Llewellyn, P.; Daturi, M.; Filinchuk, Y.; Leynaud, O.; Barnes, P.; Férey, G. *Adv. Mater.* **2007**, *19*, 2246−2251.

(15) (a) Liu, B.; Li, Y.; Hou, L.; Yang, G.; Wang, Y.-Y.; Shi, Q.-Z. *J. Mater. Chem. A* **2013**, *1*, 6535−6538. (b) Mulfort, K.; Farha, O.; Malliakas, C.; Kanatzidis, M.; Hupp, J. *Chem.—Eur. J.* **2010**, *16*, 276−281.

(16) (a) Thallapally, P. K.; Tian, J.; Radha Kishan, M.; Fernandez, C. A.; Dalgarno, S. J.; McGrail, P. B.; Warren, J. E.; Atwood, J. L. *J. Am. Chem. Soc.* **2008**, *130*, 16842−16843. (b) Walton, K. S.; Millward, A. R.; Dubbeldam, D.; Frost, H.; Low, J. J.; Yaghi, O. M.; Snurr, R. Q. *J. Am. Chem. Soc.* **2008**, *130*, 406−407.

(17) Altomare, A.; Cascarano, G.; Giacovazzo, C.; Guargliardi, A.; Burla, M. C.; Polidori, G.; Camalli, M. *J. Appl. Crystallogr.* **1994**, *27*, 435.

(18) Farrugia, L. J. *J. Appl. Crystallogr.* **1999**, *32*, 837.

(19) Otwinowski, Z.; Minor, W. *Methods Enzymol.* **1997**, *276*, 307−26.